Direct Observation of the Self-Association of Dilute Proteins in the Presence of Inert Macromolecules at High Concentration via Tracer Sedimentation Equilibrium: Theory, Experiment, and Biological Significance

Germán Rivas,[‡] Javier A. Fernandez,[‡] and Allen P. Minton*[,§]

Centro de Investigaciones Biológicas, CSIC, 28006 Madrid, Spain, and National Institute of Diabetes and Digestive and Kidney Diseases, National Institutes of Health, Bethesda, Maryland 20892

Received February 12, 1999; Revised Manuscript Received May 3, 1999

ABSTRACT: The technique of tracer sedimentation equilibrium [Rivas, G., et al. (1994) *Biochemistry* , 2341−2348 (*1*); Rivas, G., et al. (1996) *J. Mol. Recognit. 9*, 31−38 (*2*)] is utilized, together with an extension of the theory of sedimentation equilibrium of highly nonideal solutions [Chatelier and Minton, (1987) *Biopolymers 26*, 1097−1113 (*3*)], to characterize the thermodynamic activity and/or the state of association of a dilute, labeled macromolecular solute in the presence of an arbitary concentration of a second, unlabeled macromolecular solute. Experiments are performed on solutions of labeled fibrinogen (0.25−1 g/L) in bovine serum albumin (0−100 g/L) in the presence and absence of divalent cations (Ca^{2+}, Mg^{2+}), and on solutions of labeled tubulin (0.2−0.6 g/L) in dextran (0−100 g/L). It is found that in the absence of the divalent cations, the large dependence of the thermodynamic activity of fibrinogen on BSA concentration is well accounted for by a simple model for steric repulsion. In the presence of the cations and sufficiently large concentrations of BSA (>30 g/L), fibrinogen appears to self-associate to a weight-average molar mass approximately twice that of monomeric fibrinogen. Tubulin appears to self-associate to an extent that increases monotonically with increasing dextran concentration, reaching a weight-average molar mass almost 3 times that of the $\alpha\beta$ dimer in the presence of 100 g/L dextran. Possible biological ramifications are discussed.

It is increasingly appreciated that volume exclusion arising from the high total concentration of macromolecules in almost all physiological media ("macromolecular crowding") can have a large qualitative effect upon the equilibria and kinetics of macromolecular reactions taking place in such media (*4*). Simple geometric models for steric repulsion have predicted and/or successfully accounted for large changes in a broad variety of biochemical reaction rates and equilibria that are observed upon addition of "inert" volume-excluding macromolecules to a reaction medium (*5*, *6*). Intracellular reactions and intracellular processes thought to be sensitive to volume exclusion effects include protein folding, function-linked alterations in nucleic acid conformation, and the formation of protein and protein−nucleic acid complexes (*4*, *6*). Theory predicts that many of these changes may be attributed to a significant enhancement of macromolecular associations in the presence of high concentrations of inert macromolecules. While such enhancement has been inferred indirectly from a variety of experimental observations (see Tables 2 and 3 in ref *6*), enhanced association of a dilute macromolecular species in the presence of high concentrations of a second, concentrated species (i.e., in a crowded environment resembling that encountered in a physiological medium) has heretofore been inaccessible to direct observation.

The measurement of sedimentation equilibrium has become widely recognized as one of the most powerful methods for quantitative characterization of macromolecular associations in solution (*7*, *8*). The power of the method resides, first, in the ability of the centrifuge to discriminate between various molecular species on the basis of differences in buoyant mass (arguably the most fundamental and least ambiguous property of a given molecular species) and, second, in the rigorous thermodynamic formulation of sedimentation equilibrium. Although it has been recognized that the analysis of sedimentation equilibrium may be formally extended to take into account nonideality resulting from nonspecific, predominantly repulsive, interactions between macromolecular solutes (*3*, *9*, *10*), experimental application of the technique to characterize such repulsive interactions has been limited (*11*−*14*). Analysis of sedimentation equilibrium, extended to take nonideal behavior into account, has been previously utilized to detect weak self-association of individual proteins (myoglobin, aldolase, and ovalbumin) in highly concentrated, and hence highly nonideal, solutions of that protein (*12*, *13*).

We here present a reformulation and extension of the theory of sedimentation equilibrium of highly nonideal solutions (*3*, *9*) that is especially suited to the detection of associations of a dilute (labeled) macromolecular component in the presence of a second inert macromolecular component. Experimental measurements of sedimentation equilibrium have been carried out on two systems of biological interest:

[‡] Centro de Investigaciones Biológicas, CSIC.
[§] National Institutes of Health.

10.1021/bi990355z CCC: $18.00
Published on Web 07/02/1999

solutions containing a trace amount of labeled cell adhesion protein, fibrinogen, in various concentrations of bovine serum albumin (BSA);[1] and solutions containing a trace amount of labeled tubulin ($\alpha\beta$ dimer) in various concentrations of dextran. As interpreted by the theory presented here, these measurements clearly demonstrate enhancement of self-association of the trace component in the presence of high concentrations of the inert background component. Possible biological ramifications of these findings are discussed.

THEORY

Thermodynamic Analysis of Sedimentation Equilibrium of a Solution Mixture. Consider a solution containing a mixture of solute species with molar masses M_i and partial specific volumes $\bar{\nu}_i$, in a solvent of density ρ_o. Let this solution be centrifuged at angular velocity ω and absolute temperature T. At sedimentation equilibrium (the condition of no net flux of any species), the following fundamental relation (*10*) applies:

$$\frac{d\mu_i}{dr^2} = \frac{M_i^*\omega^2}{2RT} \tag{1}$$

where r denotes the radial position, R the molar gas constant, and M_i^* the buoyant molar mass of solute species i, given by

$$M_i^* = M_i(1 - \bar{\nu}_i\rho_o)$$

μ_i, the chemical potential of species i, is given by

$$\mu_i = \mu_i^\circ + RT \ln \gamma_i + RT \ln w_i$$

where μ_i°, γ_i, and w_i denote respectively the standard state chemical potential, the activity coefficient, and the weight/volume concentration of species i.[2]

Let us define the quantity

$$M_{k,app}^* \equiv \frac{2RT}{\omega^2} \times \frac{d \ln w_k}{dr^2} \tag{2}$$

called the *apparent buoyant molar mass* of species k. Equations 1 and 2 may be combined to yield, after some algebraic manipulation:

$$M_{i,app}^* = M_i^* - \sum_j w_j \left(\frac{\partial \ln \gamma_i}{\partial w_j}\right) M_{j,app}^* \tag{3}$$

Equation 3 clearly indicates that in order for species j to affect the equilibrium concentration gradient of species i, as manifested in $M_{i,app}^*$, there must exist a significant interaction between species i and j (i.e., the product of w_j and $\partial \ln \gamma_i/\partial w_j$ must be significantly different from 0) and a significant concentration gradient of species j (i.e., $M_{j,app}^*$ significantly different from 0).[3] In what follows we consider four special cases of eq 3 which are of particular interest to the experimenter.

Special Case 1: There are no solute species present that fulfill both of the above-specified conditions, i.e., have both a concentration sufficiently great to affect significantly the activity coefficients of any species present and a concentration gradient sufficiently great to have a value of $M_{j,app}^*$ significantly different from 0. Under such conditions, eq 3 reduces to

$$M_{i,app}^* = M_i^* \tag{4}$$

for all i.

While this solution may not be thermodynamically ideal, the solutes may be said to *sediment ideally*. The "classical" sedimentation equilibrium experiment, carried out at relatively low angular velocity on a dilute solution of a protein or nucleic acid in a buffer containing substantial concentrations of salts and other small molecules, corresponds to special case 1.

Special Case 2: There exists one and only one solute, designated species 0, having both a concentration and a concentration gradient sufficiently great to affect the apparent buoyant molar mass of any solute. Under these conditions, eq 3 reduces to

$$M_{i,app}^* = M_i^* - w_0\left(\frac{\partial \ln \gamma_i}{\partial w_0}\right) M_{0,app}^* \tag{5}$$

which may be rearranged and integrated with respect to w_0, to yield

$$\ln \gamma_i(w_0') = \int_0^{w_0'} \frac{1}{w_0} \frac{M_i^* - M_{i,app}^*(w_0)}{M_{0,app}^*(w_0)}\, dw_0 \tag{6}$$

where

$$M_i^* = \lim_{w_0 \to 0} M_{i,app}^*$$

Note that when $i = 0$, eq 5 reduces to the familiar expression applicable to a single self-interacting species (*18*):

$$M_{0,app}^* = \frac{M_0^*}{1 + w_0(\partial \ln \gamma_0/\partial w_0)}$$

Special Case 3: As in special case 2, only solute species 0 is present at a concentration and gradient sufficiently great to affect the gradients of other species. Let component T, present in trace quantity, exist as a mixture of species comprised either entirely or partially of T, and let the total concentration of T be denoted by $w_T \equiv \sum f_{T,i} w_i$, where $f_{T,i}$ is the mass fraction of component T in species i. We define an experimentally measurable quantity, called the apparent buoyant molar mass of component T, as

[1] Abbreviations: VT, virtual tracer; FITC, fluorescein-5-isothiocyanate; Fbg, fibrinogen; Hepes, *N*-(2-hydroxyethyl)piperazine-*N*′-2-ethanesulfonic acid; BSA, bovine serum albumin; GTP, guanosine triphosphate; PIPES, 1,4-piperazinediethanesulfonic acid.

[2] The reader is reminded that γ_i is a measure of the average free energy of interaction between a molecule of species i and all other solute molecules of the same and other species. Hence γ_i is a function of the concentrations of all species (*5*, *15*).

[3] Since the term *species* is used here to denote a single chemical species of specified molar mass, there is by definition no *direct* effect of species j upon M_i^*. However, there may exist direct effects of one or more species upon the concentration gradient of a *component* that is present in solution as a mixture of species (*16*, *17*); these will be considered subsequently.

$$M^*_{T,\mathrm{app}} \equiv \frac{2RT}{\omega^2} \times \frac{\mathrm{d} \ln w_T}{\mathrm{d}r^2} \tag{7}$$

Combination of eqs 3 and 7 yields, after algebraic manipulation:

$$M^*_{T,\mathrm{app}} = M^*_{\mathrm{w},T} - w_0 M^*_{0,\mathrm{app}} \frac{\sum_i f_{T,i} w_i (\partial \ln \gamma_i / \partial w_0)}{\sum_i f_{T,i} w_{T,i}} \tag{8}$$

where $M^*_{\mathrm{w},T}$ denotes the actual weight-average buoyant molar mass of T:

$$M^*_{\mathrm{w},T} \equiv \frac{\sum_i f_{T,i} w_i M^*_i}{\sum_i f_{T,i} w_i} \tag{9}$$

Models for Calculation/Evaluation of the Repulsive Interaction between Macromolecules. (A) Interaction between Rigid Proteins. Repulsive interactions are modeled using the scaled particle theory of mixtures of hard convex particles (*19*), as described previously (*15*). For the case in which only a single species of macromolecule (species 0) is present at high concentration, the general theoretical expression for $\ln \gamma_i$ reduces to

$$\ln \gamma_i = -\ln (1 - \rho_0 V_0) + [H_i S_0 + S_i H_0 + V_i] \frac{\rho_0}{(1 - \rho_0 V_0)} + [H_i^2 S_0^2 + 2 V_i H_0 S_0] \frac{\rho_0^2}{2(1 - \rho_0 V_0)^2} + [V_i H_0^2 S_0^2] \frac{\rho_0^3}{3(1 - \rho_0 V_0)^3} \tag{10}$$

where ρ_0 denotes the number density of species 0 (proportional to w_0), and H_i, S_i, and V_i denote respectively the Kihara supporting function, surface area, and volume of the equivalent convex particle representing species i. The values of H, S, and V for particles of various shapes are tabulated in (*15*).

If w_i and ρ_i are specified in units of g/L and cm^{-3} respectively, then

$$\frac{\partial \ln \gamma_i}{\partial w_0} = \frac{N_\mathrm{A}}{1000 M_i} \times \frac{\partial \ln \gamma_i}{\partial \rho_0} \tag{11}$$

where

$$\frac{\partial \ln \gamma_i}{\partial \rho_0} = \frac{V_0}{1 - \rho_0 V_0} + [H_i S_0 + S_i H_0 + V_i] \frac{1}{(1 - \rho_0 V_0)^2} + [H_i^2 S_0^2 + 2 V_i H_0 S_0] \frac{\rho_0}{(1 - \rho_0 V_0)^3} + [V_i H_0^2 S_0^2] \frac{\rho_0^2}{(1 - \rho_0 V_0)^4} \tag{12}$$

(B) Interaction between a Globular Protein and a "random coil" Polymer. Repulsive interactions are modeled using the available volume theory of Ogston (*20*), in which a protein of species i is modeled as a hard sphere of radius r_i and the polymer (species 0) as a random matrix of hard rods with radius r_0 and a specific exclusion volume of υ_0. According to this model:

$$\ln \gamma_i = \left(1 + \frac{r_i}{r_0}\right)^2 \upsilon_0 w_0 \tag{13}$$

and

$$\frac{\partial \ln \gamma_i}{\partial w_0} = \left(1 + \frac{r_i}{r_0}\right)^2 \upsilon_0 \tag{14}$$

The "Virtual Tracer" Approximation. Equation 8 provides a thermodynamically exact relationship between an experimentally measureable quantity, $M^*_{T,\mathrm{app}}$, and $M^*_{\mathrm{w},T}$, the weight-average molar mass of a trace solute component. However, evaluation the rightmost term in this equation requires a detailed model for the interaction between each tracer-containing species and the dominant species 0. If no information is available *a priori* about the size and shape of these species, this term would seem to present a formidable obstacle to the use of eq 9 for the analysis of experimental data. We therefore adopt the following approximation:

$$\frac{\sum_i f_{T,i} w_i (\partial \ln \gamma_i / \partial w_0)}{\sum_i f_{T,i} w_i} \simeq \frac{\partial \ln \gamma_{\mathrm{VT}}}{\partial w_0} \tag{15}$$

The left-hand side of eq 15 represents the weight-average value of $\partial \ln \gamma_i / \partial w_0$ over all species containing tracer. For the purposes of calculating the right-hand side via one of the models presented in the previous section, we define a single species of virtual tracer (VT) with molar mass equal to the weight-average molar mass of all species of actual tracer and, in the absence of independent structural information, a shape similar to that assumed for the monomeric species of tracer.[4] Combination of eqs 8 and 15 yields the final approximate result:

$$M^*_{T,\mathrm{app}} \simeq M^*_{\mathrm{w},T} - w_0 M^*_{0,\mathrm{app}} \frac{\partial \ln \gamma_{\mathrm{VT}}}{\partial w_0} \tag{16}$$

The validity of this approximate equation, which is central to the analysis of much of the experimental data reported here, was tested by simulation as described in Appendix 1. Under conditions similar to those encountered in the experimental study reported here, eqn 16 was found to be accurate to a precision of better than 10%.

MATERIALS AND METHODS

Sedimentation Equilibrium of Fibrinogen−BSA Mixtures

Materials. $Na^{125}I$ was from Amersham Corp., and Iodobeads were from Pierce Chemical Corp. The chromophore fluorescein-5-isothiocyanate (FITC) was obtained from Molecular Probes Inc. All other chemicals were of analytical grade (Merck and Sigma). Human fibrinogen (Fbg) was obtained from Kabi or from Sigma. In both cases, it was

[4] A similar approximation was made earlier by (*3*).

more than 90% clottable. Further purification was done according to (*21*) followed by gel filtration through Sephacryl S-400 HR (Amersham Pharmacia) in phosphate buffer (50 mM sodium phosphate, 150 mM NaCl, 1 mM EDTA, pH 7.0). Bovine albumin was obtained from Sigma as a lyophilized powder (minimum 99% pure), essentially fatty acid and globulin free. The proteins were equilibrated in 25 mM Hepes/HCl, 150 mM NaCl, pH 7.4, with either 0.1 mM EDTA (Hepes−EDTA buffer) or 1 mM $CaCl_2$ and 1 mM $MgCl_2$ (Hepes−Ca buffer).

Labeling Procedures. FITC labeling of Fbg was done essentially as described by (*22*). BSA was labeled with FITC according to (*23*). The degree of labeling was less than 4 mol FITC/mol of protein in all cases. Iodination of Fbg was performed as described by (*24*). Specific activity was $(1-10) \times 10^9$ cpm/mg of Fbg.

Tracer Sedimentation Equilibrium. Experiments to characterize the effect of BSA on the state of association of Fbg were performed essentially as described in (*2*). Solutions were prepared in Hepes−EDTA or Hepes−Ca buffer containing chromophorically or radioisotopically labeled Fbg at low concentration, and BSA over a broad range of concentrations ($\leq$100 g/L).

In the case of FITC-Fbg, solution samples of ca. 1 mm column length were centrifuged to sedimentation equilibrium at 6000 rpm and 20 °C in a XL-A Optima analytical ultracentrifuge (Beckman Instruments Inc.) using either double-sector or six-channel 12 mm epon centerpieces. After sedimentation equilibrium was attained (elapsed time >24 h), absorbance gradients were measured at 495−500 nm, where BSA does not absorb. In parallel, absorbance gradients of unlabeled BSA at the same BSA concentrations were measured at 300−310 nm in 3 mm double sector cells, and absorbance gradients of trace-labeled FITC-BSA were measured at 495 nm in 12 mm double sector cells. Estimates of the buoyant molar mass of each species were obtained using the programs XLAEQ or EQASSOC (Beckman Instruments; see ref *25*), and converted to molar mass using values of the partial specific volume obtained from (*26*).

When iodinated Fbg was used in the mixtures, 70 μL samples were centrifuged to sedimentation equilibrium at 6000 rpm in a preparative ultracentrifuge. Gradients of trace radiolabel and total protein (e.g., BSA) were obtained via fractionation of tube contents with the BRANDEL FR-115 centrifuge tube microfractionator (*1*, *2*, *27*). The ^{125}I-Fbg gradient was obtained via scintillation counting of fractions, and the BSA gradient was determined in separate tubes using a colorimetric protein assay (Bio-Rad). The equilibrium gradient of tracer was analyzed as described in (*1*, *2*) to yield the apparent weight-average molar mass.

Sedimentation Equilibrium of Tubulin−Dextran Mixtures

Materials. The chromophore tetramethylrhodamine succinimidyl ester was purchased from Molecular Probes. Dextran T10 (M_w 10 000) was from Pharmacia. GTP (dilithium salt) was from Boehringer. The rest of the chemicals were of analytical grade (Merck). Tubulin was prepared from calf brain by the modified Weisenberg procedure (*28*, *29*, *30*), stored in liquid nitrogen, and equilibrated in the desired buffer before use. The chromophoric labeling of tubulin in the assembled form (as microtubules) was based on the protocols described by (*31*, *32*) using a phosphate/glycerol assembly buffer (10 mM phosphate, 1 mM EGTA, 6 mM $MgCl_2$, 3.4 M glycerol, 1 mM GTP, pH 6.9). The equilibrium buffer was 100 mM PIPES, 0.1 mM EGTA, 1 mM $MgCl_2$, 0.1 mM GTP, pH 6.5 (PIPES buffer).

Tracer Sedimentation Equilibrium. Sedimentation equilibrium of chromophorically labeled tubulin was performed in solutions containing various concentrations of dextran as described above, except that the final speed was 12 000 rpm,[5] the temperature was 10 °C (to prevent tubulin assembly), and the absorbance gradient was measured at 550 nm. Solutions of dextran at the same loading concentrations were centrifuged separately to sedimentation equilibrium in preparative ultracentrifuges and the equilibrium gradients measured via microfractionation together with measurement of dextran concentration in each fraction using the anthrone colorimetric method (*34*) to determine total sugar content.

RESULTS

Fibrinogen in BSA. Typical equilibrium gradients of labeled fibrinogen in various concentrations of BSA (Hepes-EDTA buffer) are plotted in Figure 1A,B, together with the respective calculated best fits of the integrated form of eq 7:

$$s_X(r) = s_X(r_0) \exp\left[\frac{M^*_{X,\mathrm{app}}}{2RT}(r^2 - {r_0}^2)\right] \qquad (17)$$

where s_X is the signal proportional to w_X and r_0 is an arbitrarily selected reference position. The combined results are plotted as the dependence of $M^*_{X,\mathrm{app}}$ (X = Fbg or BSA) upon w_{BSA} in Figure 2 (top and bottom panels, respectively).

We first call attention to the fact that the dependence of $M^*_{\mathrm{BSA,app}}$ upon w_{BSA} reported here agrees well, over the entire range of the present study, with that reported earlier by (*13*) measured at similar pH, temperature, and ionic strength, but using a different experimental method altogether.

It is also important to note that, to within experimental precision, the values of $M^*_{\mathrm{Fbg,app}}$ obtained from gradients of FITC-labeled and ^{125}I-labeled Fbg have the same dependence upon w_{BSA} over the entire range of BSA concentrations examined, as well as the same value in the limit of $w_{\mathrm{BSA}} = 0$. Since the methods of acquiring these results are entirely different for the two labels, the close agreement between the two sets of results speaks strongly in favor of the validity of both of the techniques used here as well as the results obtained.

The dependence of $M^*_{\mathrm{BSA,app}}$ and $M^*_{\mathrm{Fbg,app}}$ (in Hepes−EDTA buffer) upon w_{BSA} may be well described empirically by the following linear relationships:

$$M^*_{\mathrm{BSA,app}}/1000 = 17.81 - 0.0845 w_{\mathrm{BSA}} \qquad (18)$$

$$M^*_{\mathrm{Fbg,app}}/1000 = 93.49 - 0.416 w_{\mathrm{BSA}} \qquad (19)$$

A variety of experimental results indicate that under the conditions of these experiments, BSA does not self-associate (*13*, *35*, *36*). If we similarly assume that in the absence of

[5] An overspeeding of 1 h at 32 000 rpm (*33*) was used to reduce the equilibration time to less than 5 h.

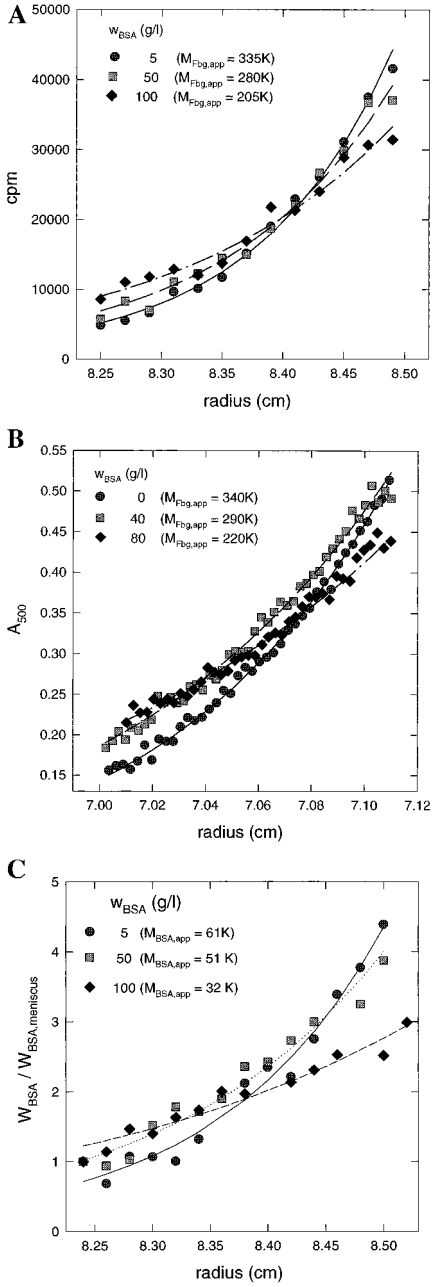

FIGURE 1: (A) Symbols: equilibrium gradients of ^{125}I-labeled fibrinogen, as measured by relative activity of radiolabel as a function of radial position, in various concentrations of unlabeled BSA. Smooth curves: gradients calculated according to eq 17, using the best-fit values of $M_{Fbg,app}$ indicated in the figure. (B) Symbols: equilibrium gradients of FITC-labeled fibrinogen, as measured by relative absorbance of FITC label as a function of radial position, in various concentrations of unlabeled BSA. Smooth curves as in (A). (C) Symbols: equilibrium gradients of unlabeled BSA obtained via colorimetric assay of radial fractions as described under Materials and Methods. Smooth curves: gradients calculated according to eq 17, using the best-fit values of $M_{BSA,app}$ indicated in the figure.

Ca^{2+} Fbg does not self-associate, then eqs 18 and 19 may be substituted into eq 6, and the resulting expressions can be integrated analytically to obtain the dependence of log γ_{BSA} and log γ_{FBG} upon w_{BSA} plotted in Figure 3 (solid lines).

The dependence of the activity coefficient of a selected solute species upon solution composition is a function of the equilibrium average interaction between a molecule of that species and all other solute molecules (*37*). Let us

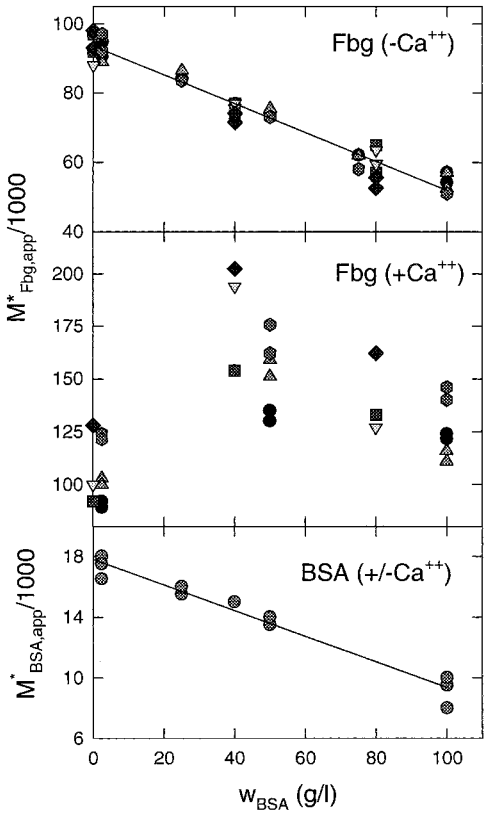

FIGURE 2: Apparent buoyant molar masses of Fbg in Hepes−EDTA buffer (top panel), Fbg in Hepes−Ca buffer (middle panel), and BSA (either buffer) as functions of BSA concentration. Fbg concentration (g/L) is indicated by symbol type: 0.25 (circles), 0.3 (squares), 0.5 (upward triangles), 0.6 (downward triangles), 0.9 (diamonds) and 1.0 (hexagons).

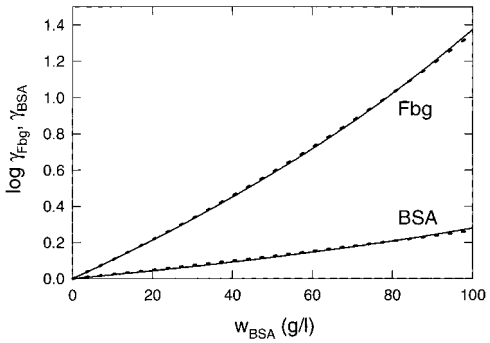

FIGURE 3: Solid lines: activity coefficients of Fbg (in Hepes−EDTA buffer) and BSA calculated from the experimental data via eq 6 as described in text. Dotted lines: best fit of of Boublík scaled particle theory to experimentally derived dependence, calculated using eq 10 with best-fit parameter values given in the text.

assume that under the conditions of the present experiments, Fbg and BSA interact primarily or entirely via steric exclusion. This assumption was tested by constructing a model in which a solution of Fbg in BSA is treated as a suspension of equivalent hard particles (see above). BSA is represented by an equivalent hard sphere of radius r_{BSA} (*5*, *35*, *36*) and Fbg by an equivalent hard spherocylinder of radius r_{Fbg} and length l_{Fbg}. First, scaled particle eq 10 was fit to the experimentally observed dependence of log γ_{BSA} upon w_{BSA} by the method of nonlinear least squares, yielding a best-fit value of $r_{BSA} = 2.7$ nm, which was held constant for subsequent calculations. Since fitting of eq 10 to the observed dependence of log γ_{Fbg} upon w_{BSA} cannot be

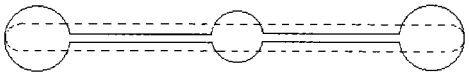

FIGURE 4: Schematic depiction of trinodular model of Fbg (*38*) (solid outline) superimposed upon spherocylindrical equivalent hard particle representing Fbg (dashed outline) yielding best fit of eq 10 to the experimentally determined dependence of Fbg activity coefficient upon BSA concentration. The lengths of the two model structures were set equal, and the cylindrical radius of the spherocylinder was allowed to vary to attain the best fit.

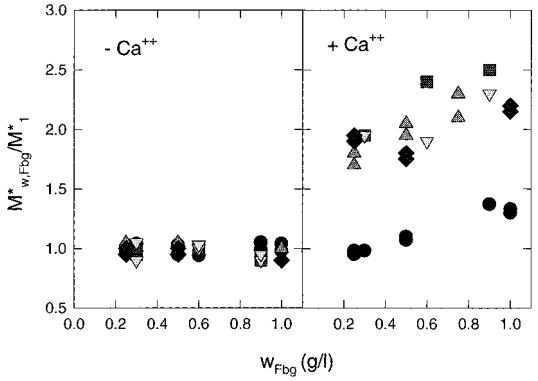

FIGURE 5: Dependence of $M^*_{w,Fbg}$ upon w_{Fbg} calculated for various concentrations of BSA in Hepes−EGTA buffer (left panel) and Hepes−Ca buffer (right panel) as described in the text. BSA concentration (g/L) is indicated by symbol type: 0 (circles), 40 (squares), 50 (upward triangles), 80 (downward triangles), and 100 (diamonds).

expected to simultaneously yield unequivocal values of either of the two highly correlated variables r_{Fbg} and l_{Fbg}, the value of l_{Fbg} was constrained equal to 47.5 nm, the length of the molecule as observed by electron microscopy (*38*). Equation 10 was then fitted with this constraint to the experimental dependence of log γ_{Fbg} upon w_{BSA}, yielding a best-fit value of $r_{Fbg} = 3.0$ nm. The calculated best-fit dependence of log γ_{BSA} and log γ_{FBG} upon w_{BSA} is plotted together with the experimental dependence in Figure 3. In Figure 4, the effective spherocylinder representing fibrinogen, that best accounts for the experimental dependence of log γ_{BSA} on w_{BSA} in the context of SPT, is overlaid on the electron microscopic model (*38*). In view of the goodness of fit of eq 10, and the similarity between the sizes and shapes of the best-fit equivalent particles and the actual protein molecules, we may safely conclude that deviations from thermodynamic ideality are due predominantly (if not entirely) to simple steric repulsion.

Rather different behavior of the tracer is observed in Hepes−Ca buffer (Figure 2, center panel). Some association of the tracer is evident even in the raw data, although quantitative interpretation requires subtraction of the effect of nonideal sedimentation. This was accomplished by defining the virtual tracer to be a spherocylinder with the same shape (axial ratio) as that determined by the best fit of SPT eq 10 to the nonassociating data obtained in Hepes−EDTA buffer, but having a mass equal to the weight-average mass of tracer. Following calculation of the tracer volume from the assumed mass and effective density, eqs 11, 12, and 16 were then used to calculate an approximate relationship between $M^*_{T,app}$ and $M^*_{T,w}$, by means of which the value of $M^*_{T,w}$ could be estimated from the measured value of $M^*_{T,app}$.

The left-hand panel of Figure 5 represents a test of internal self-consistency in the treatment of the data. Having assumed initially that Fbg does not self-associate in the absence of calcium, we calculated the dependence of the activity coefficients of both Fbg and BSA upon the concentration of BSA, and demonstrated that these dependences could be accounted for by a simple geometric model for volume exclusion (see above). Using the same geometric model together with the approximate eq 16 to relate $M^*_{Fbg,app}$ to $M^*_{w,Fbg}$ in Hepes−EDTA buffer, we demonstrate that this method of data analysis does indeed correct for nonideal sedimentation, and yields the expected result, i.e., no Fbg association in this medium.

The dependence of $M^*_{w,Fbg}$ upon w_{BSA} in Hepes−Ca buffer, calculated as described above, is plotted in the right-hand panel of Figure 5. According to eq 9, the observed increase of $M^*_{w,Fbg}$ at high BSA concentration might be attributed (in the absence of additional information) to either enhanced self-association of Fbg induced by BSA or hetero-association of Fbg and BSA. However, significant hetero-association of Fbg and BSA under the conditions of these experiments has been ruled out by the experiment described in Appendix 2. There appear to be two distinct modes of Fbg self-association: a weak self-association in the absence of BSA, which is superimposed upon a strong, saturable self-association to dimer in the presence of BSA at concentrations exceeding ca. 40 g/L.

Tubulin in Dextran. Typical equilibrium gradients of rhodamine-labeled tracer tubulin in different concentrations of dextran are plotted in Figure 6. Equation 17 was fitted to these and similar gradients, and the combined results are plotted in Figure 7. Since association of tubulin is evident upon examination of the raw data, independent information regarding the effect of dextran on the activity coefficient of tubulin is required.

Measurement of the dependence of the solubility of tubulin upon dextran concentration under similar experimental conditions (*39*) provides the following thermodynamic result applicable to solutions of trace amounts of tubulin in various concentrations of dextran:

$$\ln \gamma_{tub} = 0.038 w_{dex}(\text{g/l}) \qquad (20)$$

Equation 20 is valid for dextran concentrations up to ca. 100 g/L. We model tubulin "monomer" (actually the $\alpha\beta$ heterodimer; $M = 1 \times 10^5$) as an effective hard sphere of radius $r_{\text{"monomer"}} = 4 \times 10^{-7}$ cm; such a sphere has a radius of gyration of 3.1×10^{-7} cm, equal to that measured via small-angle X-ray scattering (*40*). By setting equal the right-hand sides of model eq 13 and experimental eq 20, and substituting in the value of $r_{\text{"monomer"}}$ assumed above, one obtains a relation between the specific exclusion volume and effective hard rod radius of dextran:

$$r_0(\text{cm}) = \frac{4.0 \times 10^{-7}}{\left(\dfrac{38}{\upsilon_0(\text{cm}^3/\text{g})}\right)^{1/2} - 1} \qquad (21)$$

The results to be presented subsequently were calculated

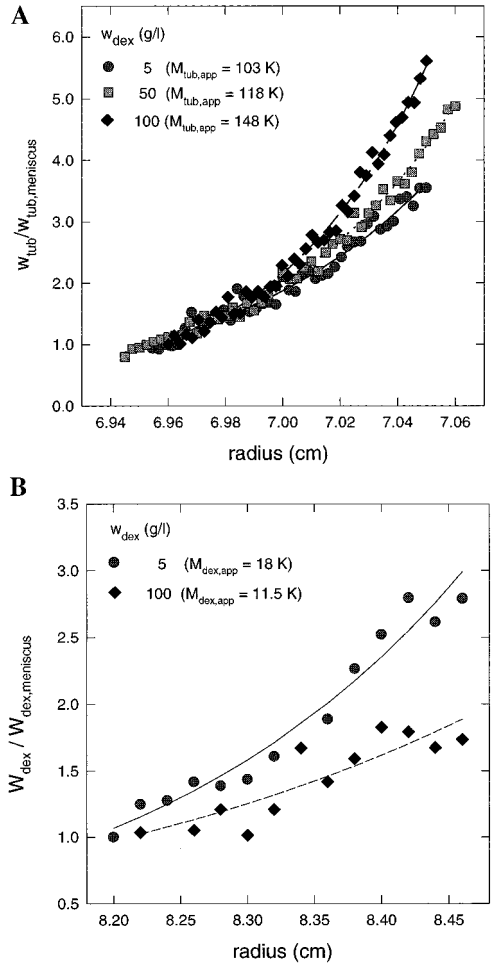

FIGURE 6: (A) Symbols: equilibrium gradients of rhodamine-labeled tubulin, as measured by relative absorbance of label, in various concentrations of unlabeled BSA. Smooth curves: gradients calculated according to eq 17, using the best-fit values of $M_{tub,app}$ indicated in the figure. (B) Symbols: equilibrium gradients of dextran, measured as described under Materials and Methods, at different dextran loading concentrations. Smooth curves: gradients calculated according to eq 17, using the best-fit values of $M_{dex,app}$ indicated in the figure.

using $\upsilon_0 = 0.8$ cm^3/g and $r_0 = 6.75 \times 10^{-8}$ cm, satisfying eq 21.[6]

In accordance with the virtual tracer approximation described above, it is assumed that the virtual tracer particle is a hard sphere with mass equal to the weight-average mass of tracer; i.e., $r_{VT} = r_{\text{“monomer”}} \times (M_{w,tub}/M_{\text{“monomer”}})^{1/3}$. Equations 14 and 16 are then used to estimate the relationship between the experimentally measured quantities $M^*_{tub,app}$ and $M^*_{w,tub}$.

The dependence of $M^*_{w,tub}$ upon w_{tub}, estimated as described above, is plotted for different dextran concentrations in Figure 8. It is evident that in the absence of dextran, tubulin does not self-associate under the conditions of these experiments.

[6] Neither r_0 nor υ_0 can be independently specified. However, we have found that the value of $\partial \ln \gamma_{VT}/\partial w_{dex}$ calculated using eq 14 with different pairs of $\{r_0, \upsilon_0\}$ satisfying eq 21 is almost independent of the particular pair of values of $\{r_0, \upsilon_0\}$ chosen, so long as υ_0 is in the range 0.6−1.0 cm^3/g, and the corresponding values of r_0 are thus in the range (5.5−8.0) $\times$ 10^{-8} cm. By fitting the Ogston model to data on the partitioning of a variety of macrosolutes between bulk solution and dextran gels, Laurent and Killander (*41*) obtained a comparable value of $r_0 = 7 \times 10^{-8}$ cm.

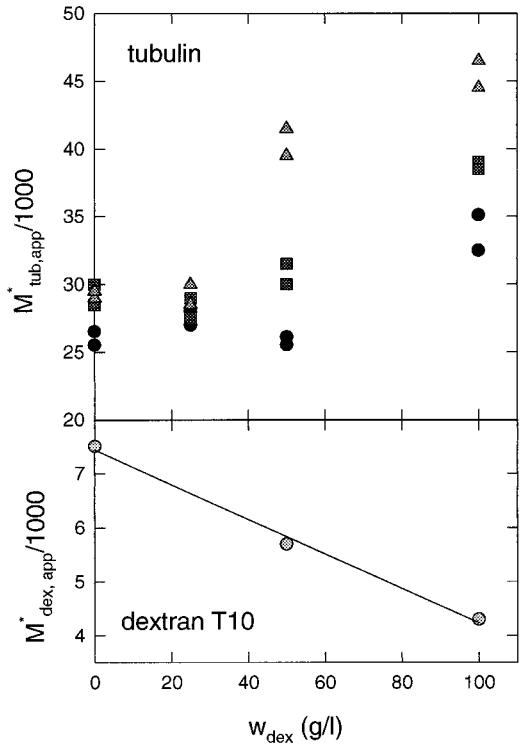

FIGURE 7: Dependence of experimentally determined $M^*_{tub,app}$ (upper panel) and $M^*_{dex,app}$ (lower panel) upon dextran concentration. Tubulin concentration (g/L) is indicated by symbol type: 0.2 (circles), 0.4 (squares), 0.6 (triangles).

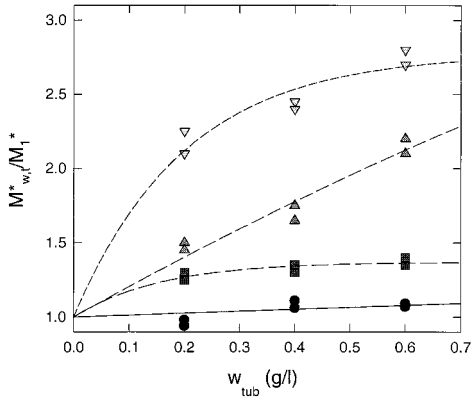

FIGURE 8: Dependence of $M^*_{w,tub}$ upon w_{tub}, calculated for different concentrations of dextran as described in text. Dextran concentration (g/L) is indicated by symbol type: 0 (circles), 25 (squares), 50 (upward triangles), and 100 (downward triangles). Curves are fits of smooth empirical (rectangular hyperbolic) functions.

However, the weight-average molar mass of tubulin increases monotonically with increasing dextran and tubulin concentration. In principle, this could be due either to tubulin self-association or to tubulin−dextran hetero-association. However, hetero-association of dextran and tubulin would imply an attractive, stabilizing interaction between the two components that would act to solubilize tubulin, contradicting the experimental observation that dextran reduces the solubility of tubulin (see above). Hence, we conclude that dextran is facilitating the formation of soluble oligomers of tubulin under nonassembly conditions.

DISCUSSION

In the present study we have extended theoretical results previously obtained by (*3*) and experimental techniques

previously developed and utilized by (*1*) and (*2*) in order to characterize the state of association of a labeled protein, present at trace concentrations ("tracer"), in a solution of another, unlabeled, macromolecular component at arbitrary concentration ("crowder"). Solutions such as these exhibit excluded volume effects comparable to those encountered in biological media.

For the case of noninteracting components, exemplified in the present study by labeled Fbg in Ca^{2+}-free BSA, the method has been shown to yield a quantitative, model-independent determination of the dependence of the thermodynamic activity of both tracer and crowder on the concentration of crowder. In the case of an associating tracer (labeled Fbg in BSA + Ca^{2+}, labeled tubulin in dextran), the method has been shown to yield a robust quantitative estimate of the extent of association of the tracer that is only weakly dependent upon the choice of a model for repulsive interaction between tracer and crowder and the values of model parameters. Given independent information about the nature of the repulsive interaction, the resulting estimate appears to be valid to within a precision of better than 10%, certainly adequate for semiquantitative analysis of the deduced pattern of association.

Sedimentation equilibrium is one of three classical methods for the direct measurement of thermodynamic activity of macromolecules in solution, the other two being measurement of osmotic pressure and Rayleigh scattering of light (*18*). However, neither of these techniques appears suitable for the measurement of the activity and state of association of a trace macromolecule in a solution of a macromolecular crowder. We believe that the method and analysis presented is uniquely capable of providing such information, and that the information so obtained is of importance with respect to a correct understanding of biochemical equilibria and kinetics in physiological media, as elaborated below.

The dependence of the thermodynamic activity of labeled fibrinogen on the concentration of BSA in Ca^{2+}-free buffer (at moderate ionic strength) has been shown to be explicable quantitatively on the basis of a simple model, in which the molecular species are represented by hard convex particles having sizes and shapes similar to those of the the corresponding molecules viewed at low resolution. Models of this type have been shown to account well for concentration-dependent properties of solutions of proteins and other macromolecules (see ref *15* for a recent review).

We have found that at a BSA concentration of ca. 80 g/L, roughly the total concentration of protein in blood plasma[7] (*42*, *43*), the activity coefficient of dilute Fbg is approximately equal to 10. From a functional point of view, one might therefore expect soluble Fbg in blood plasma to bind to surface-immobilized binding sites (on, for example, the surface of a platelet) with an affinity that is significantly greater, perhaps by as much as an order of magnitude, than that measured in a buffer of similar pH and ionic strength, but lacking the "inert" proteins (see Section II of ref *44*). It is suggested that the influence of volume-excluding "inert" macromolecules upon the thermodynamic activity of fibrinogen, and perhaps other cell adhesion proteins, be taken into account in the design and optimization of in vitro assays for platelet antagonists (*45*, *46*, *47*).

[7] The concentration of albumin alone in blood plasma is ca. 50 g/L.

Also of possible physiological relevance is the observation that in Hepes−Ca buffer, which contains Ca^{2+} and Mg^{2+} at roughly the same concentrations found in whole blood (*42*, *43*), and BSA concentrations exceeding 40 g/L, the weight-average molar mass of trace Fbg corresponds to 2 or more times that of monomeric Fbg. We therefore suspect that the dominant state of association of Fbg in blood plasma may not be monomeric, and a comparable study conducted in actual plasma or protein-containing plasma-like media is strongly indicated. This finding may bear upon our understanding of the mechanism of hemostasis (*48*, *49*), particularly in light of prior reports that high concentrations of unrelated proteins substantially accelerate the formation of fibrin clots (*50*, *51*), and that addition of albumin reduces the solubility of fibrin/fibrinogen complexes (*52*).

The observation that significant concentrations of dextran, a presumably inert polymer, facilitate the formation of soluble oligomers of tubulin under nonassembly conditions accords well with reports (*39*, *53*) that dextran facilitates the formation of microtubules under assembly conditions. It has been reported (*54*), and we have confirmed (data not shown), that addition of small molecule cosolutes, such as glutamate, that are known to facilitate the formation of microtubules under assembly conditions, also facilitates the formation of soluble oligomers of tubulin under nonassembly conditions. These combined observations suggest the possibility that soluble oligomers of tubulin may be precursors to, and/or significant intermediates in the formation of, large insoluble arrays of tubulin, including, but not limited to, microtubules (*55*).

Although we have not yet attempted to analyze the derived dependence of tracer self-association upon the concentration of tracer in the context of reaction schemes for equilibrium self-association, we note that such schemes should be relatively simple to model for the following reason. Let the thermodynamic equilibrium association constant for formation of the *i*th species of tracer be defined as

$$K^o_{Ti} \equiv \frac{a_{Ti}}{a^i_{T1}} = \frac{\gamma_{Ti}}{\gamma^i_{T1}} \times \frac{w_{Ti}}{w^i_{T1}} \tag{22}$$

At a fixed concentration of crowder, the activity coefficients of all species of tracer depend only upon the concentration of crowder, i.e., independent of the concentration of any species of tracer. The apparent equilibrium association constant for formation of the *i*th species of tracer, defined in terms of concentrations rather than activities, is given by

$$K_{Ti} \equiv \frac{w_{Ti}}{w^i_{T1}} = K^o_{Ti}\Gamma \tag{23}$$

where

$$\Gamma \equiv \frac{\gamma^i_{T1}}{\gamma_{Ti}}$$

Since Γ is constant at a fixed concentration of crowder, it follows that K_{Ti} is likewise a constant at fixed concentration of crowder, and may thus be legitimately used to model self-association in such a solution, even though the solution may be highly thermodynamically nonideal. Information about

the nonideal repulsive interaction between the crowder and each of the association states of tracer could in principle be extracted from the dependence of the values of the individual K_{Ti} upon the concentration of crowder.

APPENDIX 1: NUMERICAL TEST OF THE "VIRTUAL TRACER" APPROXIMATION

The following exercise was undertaken in order to explore the feasibility of using approximate eq 16 to evaluate the true buoyant weight-average molar mass of tracer, $M^*_{w,T}$, from the experimentally measured apparent buoyant molar masses of tracer and crowder, $M^*_{T,app}$ and $M^*_{0,app}$, in the absence of information regarding the relative abundance, size, and shape of molecular species containing tracer. For a given preselected value of $M_{w,T}/M_1$, a broad variety of model (simulated) distributions of tracer with that particular value of $M_{w,T}/M_1$ were generated, such that for each model distribution the molar mass (and therefore buoyant molar mass), relative abundance, size, and shape of each tracer-containing species are specified. (It is assumed throughout that the crowder consists of a single species of known size and shape.) Thus, for each model distribution, given the experimentally determined dependence of $M^*_{0,app}$ on w_0, one can precisely calculate $\ln \gamma_i$ and $\partial \ln \gamma_i/\partial w_0$ for all i (eqs 10−12 or eqs 13 and 14), and $M^*_{T,app}$ (eq 8). Next, for identical values of $M_{w,T}/M_1$ and w_0, the value of $M^*_{T,app}$ was calculated using the virtual tracer approximation as described below, and the result was compared to that of the exact calculation based upon knowledge of the distribution of molecular species.

Fbg in BSA. When species 0 is a globular protein, the equivalent particle is defined to be a hard sphere of volume determined by the specified molar mass and specific exclusion volume. Subsequent calculations of $\partial \ln \gamma_i/\partial w_0$ are carried out using eqs 11 and 12. A variety of arbitrary ensembles (mass distributions) of tracer species represented by hard spherocylinders of specified volumes and axial ratios, subject to the condition $M_{w,T} = 2M_1$,[8] were created. For each of these ensembles, the virtual tracer was defined as in the text, i.e., as a hard spherocylinder having a volume equal to the mass-average volume of tracer particles in the ensemble, and an axial ratio equal to that of the monomeric species of tracer. Then the values of the left-hand side and the right-hand side of eq 16 were independently calculated as a function of w_0 up to a maximum value of $w_o = 100$ g/L. It was found that so long as no significant tracer species had an axial ratio differing from that of monomer by more than a factor of 2, the approximate eq 16 was accurate to within 10%.[9]

Tubulin in Dextran. When species 0 is a polymer, the effective particle is defined to be a hard rod of specified radius and exclusion volume, and subsequent calculations of $\partial \ln \gamma_i/\partial w_0$ are carried out using eq 14. A variety of ensembles of hard spherical tracer particles with arbitrarily chosen distributions of mass (and volume), with no limitation on the value of $M_{w,T}$, were created. For each of these ensembles, the validity of approximate eq 16 was tested as described above. It was found that for all ensembles tested, eq 16 estimated the value of $M_{w,T}$ to a precision of better than 2%.

APPENDIX 2: TEST FOR HETERO-ASSOCIATION OF FIBRINOGEN AND BSA IN THE PRESENCE OF DIVALENT CATIONS

A solution mixture containing 10 g/L Fbg, 80 g/L BSA, and a trace amount of ^{125}I-BSA was incubated at 20 °C in Hepes−Ca buffer. An aliquot of the solution was removed for subsequent measurement of specific radioactivity. The solution was centrifuged in a TL100 rotor at 100 000 rpm for 60 min. Under these conditions, Fbg is pelleted into the bottom 10% of the tube. Following centrifugation, a second aliquot of volume equal to the first was removed from the top of the solution. The fractional reduction in radioactivity near the solution meniscus following pelleting of Fbg was 1.2% (mean of four replicates). If it is assumed that the observed depletion was due to sedimentation of Fbg-bound BSA, then the extent of depletion corresponds to 0.5 mol of BSA bound/mol of Fbg. In order to account for the increase of $M^*_{w,Fbg}$ observed in the presence of high concentrations of BSA (results shown in the right panel of Figure 5) on the basis of hetero-association of Fbg and BSA, it is necessary to postulate an average value of 5−7 mol of BSA bound/mol Fbg at significantly lower concentrations of both Fbg and BSA. The results of the depletion experiment described here thus demonstrate that the formation of Fbg−BSA complexes cannot account for more than a very small percentage of the increase in $M^*_{w,Fbg}$ observed in the presence of BSA. This increase must therefore be attributed almost entirely to self-association of Fbg.

ACKNOWLEDGMENT

We thank Jose-Manuel Andreu (CIB, CSIC), Jose González-Rodríguez (Rocasolano Institute, CSIC), and Peter Schuck (NIH) for helpful advice and for critically reviewing early drafts of this paper.

REFERENCES

1. Rivas, G., Ingham, K. C., and Minton, A. P. (1994) *Biochemistry 33*, 2341−2348.
2. Rivas, G., Tangemann, K., Minton, A. P., and Engel, J. (1996) *J. Mol. Recognit. 9*, 31−38.
3. Chatelier, R. C., and Minton, A. P. (1987) *Biopolymers 26*, 1097−1113.
4. Minton, A. P. (1997) *Curr. Opin. Biotechnol. 8*, 65−69.
5. Minton, A. P. (1983) *Mol. Cell. Biochem. 55*, 119−140.
6. Zimmerman, S. B., and Minton, A. P. (1993) *Annu. Rev. Biophys. Biomol. Struct. 22*, 27−65.
7. Harding, S. E., Rowe, A. J., and Horton, J. C., Eds. (1992) *Analytical Ultracentrifugation in Biochemistry and Polymer Science*, Royal Society of Chemistry, Cambridge.

[8] This restriction was established to limit the number of parameters subject to variation, while maintaining the similarity of the test value of $M_{w,T}$ to that calculated from the experimental results reported in the text.

[9] The worst case result was obtained for the ensemble consisting of 50% monomer of axial ratio 6.5 and 50% trimer of axial ratio 19 (modeling a strictly linear aggregate of three fibrinogen molecules), for which eq 16 with a virtual tracer with $L = 6.5$ calculated a value of $M_{w,T}$ at $w_0 = 100$ g/L that was 25% too high. Such an aggregate is considered highly improbable, as fibrin clot formation is thought to proceed from fibrils constructed of staggered side-to-side pairs of fibrin protomers (*56*). A trimer of fibrinogen molecules constructed in this fashion would be most appropriately modeled by a spherocylinder with an axial ratio of $\sqrt{2}$ times that of the monomer, as it would have approximately twice the length and twice the cross-sectional area.

8. Schuster, T. M., and Laue, T. M., Eds. (1994) *Modern Analytical Ultracentrifugation*, Birkhäuser, Boston, MA.
9. Chatelier, R. C., and Minton, A. P. (1987) *Biopolymers 26*, 507−524.
10. Wills, P. R., and Winzor, D. J. (1992) in *Analytical Ultracentrifugation in Biochemistry and Polymer Science* (Harding, S., Rowe, A., and Horton, J., Eds.) pp 311-330, Royal Society of Chemistry, Cambridge.
11. Ross, P. D., Briehl, R. W., and Minton, A. P. (1978) *Biopolymers 17*, 2285−2288.
12. Minton, A. P., and Lewis, M. S. (1981) *Biophys. Chem. 14*, 317−324.
13. Muramatsu, N., and Minton, A. P. (1989) *J. Mol. Recogn. 1*, 166−171.
14. Wills, P. R., Georgalis, Y., Dijk, J., and Winzor, D. J. (1995) *Biophys. Chem. 57*, 37−46.
15. Minton, A. P. (1998) in *Energetics of Biological Macromolecules Part B* (Ackers, G., and Johnson, M., Eds.) Vol. 295, pp 127−149, Academic Press, San Diego.
16. Hsu, C. S., and Minton, A. P. (1991) *J. Mol. Recogn. 4*, 93−104.
17. Minton, A. P. (1997) *Prog. Colloid Polym. Sci. 107*, 11−19.
18. Tanford, C. (1961) *Physical Chemistry of Macromolecules*, John Wiley and Sons, New York.
19. Boublík, T. (1974) *Mol. Phys. 27*, 1415−1427.
20. Ogston, A. G. (1958) *Trans. Faraday Soc. 54*, 1754−1757.
21. Laki, K. (1951) *Arch. Biochem. Biophys. 32*, 317−324.
22. Xia, Z., Liu, Q., Kasirer-Friede, A., Brown, E., and Frojmovic, M. M. (1996) *Br. J. Haematol. 93*, 204−214.
23. Waggoner, A. (1995) *Methods Enzymol. 246*, 362−373.
24. Parise, L. V., and Phillips, D. R. (1985) *J. Biol. Chem. 260*, 10698−10707.
25. Minton, A. P. (1994) in *Modern Analytical Ultracentrifugation* (Schuster, T. M., and Laue, T. M., Eds.) pp 81−93, Birkhauser, Boston.
26. Durchschlag, H. (1986) in *Thermodynamic Data for Biochemistry and Biotechnology* (Hinz, H. J., Ed.) pp 45−128, Springer-Verlag, Berlin.
27. Darawshe, S., Rivas, G., and Minton, A. P. (1993) *Anal. Biochem. 209*, 130−135.
28. Weisenberg, R. C., Borisy, G. G., and Taylor, E. W. (1968) *Biochemistry 7*, 4466−4479.
29. Lee, J. C., Frigon, R. P., and Timasheff, S. N. (1973) *J. Biol. Chem. 248*, 7253−7262.
30. Díaz, J. F., and Andreu, J. M. (1993) *Biochemistry 32*, 2747−2755.
31. Mejillano, M. R., and Himes, R. H. (1989) *Biochemistry 28*, 6518−6524.
32. Hyman, A., Drechsel, D., Kellogg, D., Salser, S., Sawin, K., Steffen, P., Wordeman, L., and Mitchison, T. (1991) *Methods Enzymol. 196*, 478−485.
33. Sackett, D. L., and Lippoldt, R. E. (1991) *Biochemistry 30*, 3511−3517.
34. Loewus, F. A. (1952) *Anal. Chem. 24*, 219.
35. Minton, A. P., and Edelhoch, H. (1982) *Biopolymers 21*, 451−458.
36. Minton, A. P. (1995) *Biophys. Chem. 57*, 65−70.
37. Hill, T. L. (1960) *Introduction to Statistical Thermodynamics*, Addison-Wesley, Reading, MA.
38. Hall, C. E., and Slayter, H. S. (1959) *J. Biochem. Biophys. Cytol. 5*, 11−15.
39. García Alvarez, B. (1998) in *Facultad de Quimica (Dept. Bioquím. and Biol. Mol. I)* p 54, Complutense Univ., Madrid.
40. Bordas, J., Mandelkow, E. M., and Mandelkow, E. (1983) *J. Mol. Biol. 164*, 89−135.
41. Laurent, T. C., and Killander, J. (1964) *J. Chromatogr. 14*, 317−330.
42. Dittmer, D. S., Ed. (1961) *Blood and other body Fluids*. *Biological Handbooks*, FASEB, Washington, DC.
43. Bing, D. H., Ed. (1979) *The Chemistry and Physiology of the Human Plasma Proteins*, Pergamon Press, New York.
44. Minton, A. P. (1994) in *Cellular and molecular physiology of cell volume regulation* (Strange, K., Ed.) pp 181−190, CRC Press, Boca Raton.
45. Nichols, A. J., Ruffolo, R. R., Huffman, W. F., Poste, G., and Samanen, J. (1992) *Trends Pharmacol. Sci. 13*, 413−417.
46. Coller, B. (1992) *Annu. Rev. Med. 43*, 171−180.
47. Coller, B. (1997) *J. Clin. Invest. 99*, 1467−1471.
48. Ruggeri, Z. M. (1993) *Curr. Opin. Cell Biol. 5*, 898−906.
49. Du, X., and Ginsberg, M. H. (1997) *Thromb. Haemostasis 78*, 96−100.
50. Wilf, J., Gladner, J. A., and Minton, A. P. (1985) *Thromb. Res. 37*, 681−688.
51. Torbet, J. (1986) *Biochemistry 25*, 5309−5314.
52. Galanakis, D. K. (1995) *Thromb. Res. 78*, 303−313.
53. Herzog, W., and Weber, K. (1978) *Eur. J. Biochem. 91*, 249−254.
54. Foster, K. E., and Rosemeyer, M. A. (1986) *FEBS Lett. 194*, 78−84.
55. Kirchner, K., and Mandelkow, E. M. (1985) *EMBO J. 4*, 2397−2402.
56. Fowler, W. E., Hantgan, R. R., Hermans, J., and Erickson, H. P. (1981) *Proc. Natl. Acad. Sci. U.S.A. 78*, 4872−4876.

BI990355Z